Electrospun cellulose acetate composites containing supported metal nanoparticles for antifungal membranes

Please, cite as follows:

Jennifer Quirós, Soledad Gonzalo, Blanca Jalvo, Karina Boltes, José Antonio Perdigón-Melón, Roberto Rosal. Electrospun cellulose acetate composites containing supported metal nanoparticles for antifungal membranes, Science of The Total Environment, Volumes 563–564, 2016, Pages 912-920, https://doi.org/10.1016/j.scitotenv.2015.10.072

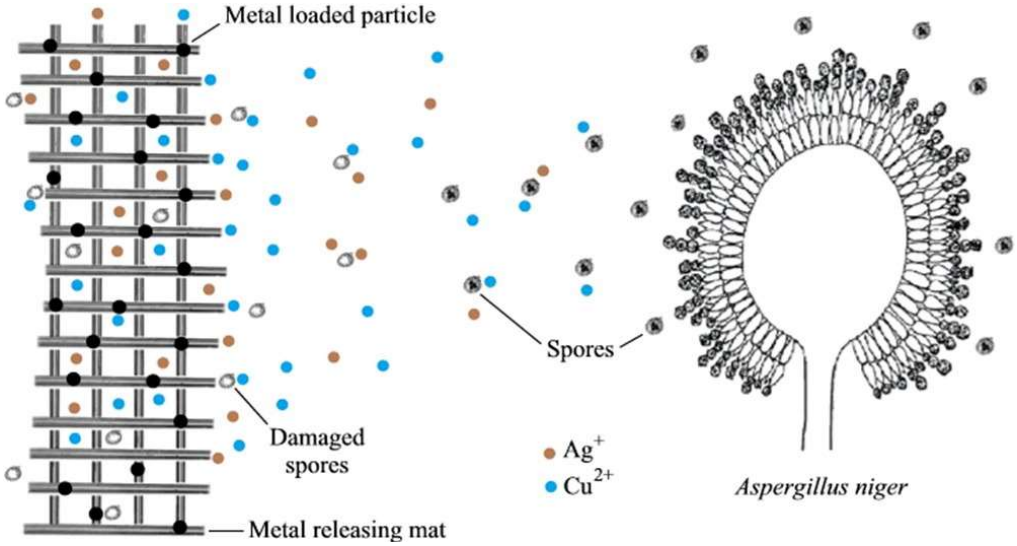

https://www.sciencedirect.com/science/article/pii/S0048969715308846

Electrospun cellulose acetate composites containing supported metal nanoparticles for antifungal membranes

Jennifer Quirós, Soledad Gonzalo, Blanca Jalvo, Karina Boltes, José Antonio Perdigón-Melón, Roberto Rosal*

Department of Chemical Engineering, University of Alcalá, Alcalá de Henares, Madrid 28871, Spain

* Corresponding author: roberto.rosal@uah.es

Abstract

Electrospun cellulose acetate composites containing silver and copper nanoparticles supported in sepiolite and mesoporous silica were prepared and tested as fungistatic membranes against the fungus *Aspergillus niger*. The nanoparticles were in the 3–50 nm range for sepiolite supported materials and limited by the size of mesopores (5–8 nm) in the case of mesoporous silica. Sepiolite and silica were well dispersed within the fibers, with larger aggregates in the micrometer range, and allowed a controlled release of metals to create a fungistatic environment. The effect was assessed using digital image analysis to evaluate fungal growth rate and fluorescence readings using a viability stain. The results showed that silver and copper nanomaterials significantly impaired the growth of fungi when the spores were incubated either in direct contact with particles or included in cellulose acetate composite membranes. The fungistatic effect took place on germinating spores before hyphae growth conidiophore formation. After 24 h the cultures were separated from fungistatic materials and showed growth impairment only due to the prior exposure. Growth reduction was important for all the particles and membranes with respect to non-exposed controls. The effect of copper and silver loaded materials was not significantly different from each other with average reductions around 70% for bare particles and 50% for membranes. Copper on sepiolite was particularly efficient with a decrease of metabolic activity of up to 80% with respect to controls. Copper materials induced rapid maturation and conidiation with fungi splitting in sets of subcolonies. Metal-loaded nanomaterials acted as reservoirs for the controlled release of metals. The amount of silver or copper released daily by composite membranes represented roughly 1% of their total load of metals. Supported nanomaterials encapsulated in nanofibers allow formulating active membranes with high antifungal performance at the same time minimizing the risk of nanoparticle release into the environment.

Keywords: Electrospinning; Nanometals; Fungistatic membranes; Cellulose acetate; Sepiolite; Mesoporous silica

1. Introduction

Many microorganisms have developed adaptive mechanisms for colonizing surfaces causing major problems in a number of man-made materials. The biofouling is particularly important for membrane filtration processes and determines their practical application in many water and wastewater treatment processes. Electrospun nanofibers represent an emerging category of membranes that offer low weight, high permeability and tunable pore size together with unique functionalization possibilities and the potential to incorporate nanoscale chemistry (Tabe, 2014). Electrospinning is the only technique available for the production of nanofibrous membranes, which is applicable to a wide variety of dissolved or melted polymers (Greiner and Wendorff, 2007). The development of antimicrobial surfaces is a field of intense research in order to reduce or eliminate microbial attachment and biofilm formation (Krishnan et al., 2008, Hasan et al., 2013). Antibiofouling behavior is obtained by manipulating surface chemistry or topography to create unfavourable environments for cellular attachment (Campoccia et al., 2013).

Membrane bacterial biofilms have been extensively studied, but other microorganisms including fungi have been largely ignored even if the presence of a high number of different fungi strains have been identified in membrane biofilms (Baker and Dudley, 1998, Al-Ashhab et al., 2014). Fungal infections significantly contribute to morbidity and mortality (Pfaller et al., 2006, Pfaller, 2012). *Aspergillus niger* is a generally non-pathogenic fungus widely distributed in nature, but during colonization it may produce the mycotoxins ochratoxin A and fumonisins B2 and B4, which have proven carcinogenic to humans and laboratory animals (Palma et al., 2007, Mogensen et al., 2010). Abundant in man-made environments, *A. niger* is responsible for the postharvest decay of a number of crops causing high economic impact (Pitt and Hocking, 2009, Flannigan et al., 2011).

The antifungal effect of silver nanoparticles has been the subject topic of several studies with emphasis on strains of *Candida* spp. (Falletta et al., 2008, Roe et al., 2008, Panáček et al., 2009). Magnetic silver nanocomposites prepared with maghemite and magnetite have been tested for antimycotic activity using several strains of *Candida* spp. (Prucek et al., 2011). ZnO nanoparticles have been proposed based on their capacity of inducing oxidative damage (Sharma et al., 2010, Lipovsky et al., 2011). Antifungal silica

nanoparticles have been prepared containing Amphotericin B covalently immobilized on silica nanoparticles or coated with a quaternary ammonium cationic surfactant (Paulo et al., 2010, Botequim et al., 2012). Gold nanoparticles were also studied against various strains of *Candida* spp. (Wani and Ahmad, 2013), but in general much less attention has been paid to antifungal nanoparticles in comparison to antibacterial applications. The applications with free nanoparticles must tackle the problem of their possible release into the environment, which is a major concern in light of the potential risk of nanoparticles (Grieger et al., 2012). Alternatively, the attachment of nanometals to non-nano supports offers advantages regarding regulatory restraints for nanomaterials or at least reducing the probability of environmental leaching of nanoparticles (Pasricha et al., 2012). The EU definition of nanomaterial (2011/696/EU) indicates that a material containing particles with one or more external dimensions is in the size range 1–100 nm. Therefore, supporting nanoparticles in a non-nano material and embedding them into fibers circumvents possible regulatory constraints.

Electrospun nanofibers based on high molecular weight chitosan were tested against *A. niger* and *Candida albicans* (Nada et al., 2014). The grafting of styrene/maleic anhydride copolymers with poly(propylene glycol) monoamine and 5-amino-8-hydroxyquinoline was also explored as covalent post-processing for producing nanofibrous membranes against *C. albicans* (Ignatova et al., 2010). The preparation of antifungal nanofibers has been undertaken by blend electrospinning using a number of encapsulated drugs. Kim and Michielsen (2015) included and tested several antifungal photochemical dyes active due to the production of singlet oxygen grafted into electrospun nylon. Karthikeyan et al. (2015) used acrylic electrospun polymers to prepare a topical gel containing fluconazole for the treatment of infections produced by *C. albicans*. Liu et al. (2012) used coelectrospinning or blend-electrospinning of cellulose acetate and polyester urethane with inclusion of the antimicrobial agent, polyhexamethylene biguanide. Metronidazole blended into poly(vinyl alcohol)/poly(ethylene oxide) fibers produced using Nanospider technology were tested against *A. niger*, *Penicillium notatum* and *Aspergillus flavus*, with good results in terms of inhibition zone (El-Newehy et al., 2012). Other nanofibers have been developed including antifungal compounds such as clotrimazole, amidoxime and others (Sirelkhatim et al., 2015, Lakshminarayanan et al., 2014, Tonglairoum et al., 2015).

The incorporation of metals is a well-known way of enhancing the antibiofouling properties of membranes (Knetsch and Koole, 2011). Sun et al. (2011) reported the use of copper ions to increase the antimicrobial activity of epigallocatechin-3-gallate by limiting its oxidation in electrospun polyvinyl alcohol nanofibers tested against *C. albicans*. Aqueous poly(vinyl alcohol-co-vinyl acetate)/octadecyl amine-montmorillonite electrospun nanocomposites were prepared with in situ generated silver nanoparticles displaying antifungal activity against several species of the genus *Candida* (Rzayev et al., 2014). Electrospun polyacrylonitrile nanofibers externally loaded with silver nanoparticles showed excellent results for inhibiting the growth of the fungus *Monilia albicans* (Shi et al., 2015). Composite polycaprolactone nanofibers with silver particles precipitated onto their surface inhibited > 99% of the growth of *C. albicans* (Dobrzański et al., 2014). The immobilization of nanoparticles in electrospun fibers also offers a way of overcoming the tendency of nanoparticles to agglomerate in complex natural media (Xiao et al., 2009). Additionally, the polymer creates a barrier between particles and the environment allowing a controlled metal release that takes place through diffusion to the surface of fibers (Quirós et al., 2015a).

In this work, we studied the use of cellulose acetate composite fibers loaded with silver and copper nanometals supported on particles of sepiolite and mesoporous silica. The rationale was to prepare stable materials thanks to the encapsulation of metals within nanofibers by avoiding loosely attached nanoparticles that could be easily dispersed into the environment. The efficiency of metal-loaded membranes against the fungus *A. niger* was quantitatively assessed by tracking its growth after the exposure of spores and by using a fluorescent viability stain.

2. Materials and methods

2.1. Materials

Pluronic P123 (Aldrich $EO_{20}PO_{70}EO_{20}$, EO ethylene oxide, PO propylene oxide, MW = 5800) and tetraethoxysilane (TEOS 98% GC Aldrich) were used as received. Cellulose acetate (CA) was purchased from Sigma Aldrich with molecular weight ~ 50,000 g/mol and 39.7 wt.% acetyl. Acetone (≥ 99.5%) was reagent grade, obtained from Sigma Aldrich and used as received. The components of culture media were biological grade acquired from Conda-Pronadisa (Spain). Cell Stain FUN-1 was acquired from Life Technologies, Molecular Probes (Eugene, USA).

Silica SBA-15 (SBA) was prepared according to a method reported elsewhere (Rioux et al., 2005). Briefly, 6 g of Pluronic P123 were dissolved in 45 g of water and 180 g of 2 M HCl and stirred at 308 K until dissolution. TEOS (12.5 g) was slowly added and the mixture aged at 373 K for 24 h. The white powder was recovered by filtration, washed, dried at 323 K overnight and calcined for 12 h at 773 K with a heating rate of 1 K/min. The impregnation of SBA-15 was carried out by the minimum volume method. Copper (cupric nitrate trihydrate, Fluka) or silver (silver nitrate, Sigma-Aldrich) were dissolved in 30 mL of water. The solution was slowly poured over 5 g of calcined SBA-

15 while stirring. The solid was dried at 323 K overnight and calcined under air flow for 8 h at 773 K with a heating rate of 1 K/min. The metal-loaded mesoporous materials, CuO/SBA-15 (Cu/SBA) and Ag/SBA-15 (Ag/SBA), had a content of 8.9 wt.% copper (11.2 wt.% as CuO) and 3.5 wt.% silver (as Ag). The particle size of SBA and metal-loaded SBA was 1.3 ± 0.2 μm as measured by DLS in aqueous dispersion. SEM images of SBA and metal-loaded SBA can be viewed in Fig. S1 (D, E, F). The external aspect was similar in all cases with most particles roughly spherical or slightly elongated. The dimensions were near the micrometer with a few distinctive features associated to metal deposition, which are particularly visible in Fig. S1-B. Metal particles in SBA-15 prepared using incipient wetness impregnation get included in the regular channel-like pore structure of SBA-15. Metals become confined in the inner walls of SBA-15, the size of their particles being limited by the size of mesopores (5–8 nm) except for a certain amount of particles that spread on the surface of metal loaded silica (Wang et al., 2014).

Raw sepiolite (SEP) and metal-loaded sepiolite particles were produced by Tolsa S.A., Spain with a silver (Ag/SEP) and copper (Cu/SEP) content of 24.4 wt.% Ag and 18.5 wt.% Cu (23.1% as CuO) as measured by ICP-MS. The procedure for preparing metal-functionalized sepiolite was described elsewhere (Esteban-Cubillo et al., 2008, Dasari et al., 2012). Briefly, an acid lixiviation step of magnesium was performed prior to the introduction of metallic cations. The incorporation of silver or copper took place by polycondensation of metal alkoxides followed by a thermal treatment, which collapsed the sepiolite and fixed the metallic nanoparticles into the structure of the anhydrous silicate. The advantage of this process is that the nanoparticles become closely embedded in the silicate particles, rather than being loosely held. Fig. S1 (A, B, C) shows TEM images of SEP and metal-loaded SEP. Metal nanoparticles were clearly visible in loaded samples with a relatively broad nanoparticle size distribution, which ranged from 3 to 50 nm on a base material with fibrillar structure. SEP fibers had an average length of 1–2 μm, and ~ 10 nm width.

2.2. Electrospinning

CA 9 wt.% was prepared by dissolving the required amount of CA in a mixture of acetone and distilled water (80:20) followed by constant magnetic stirring for 24 h. 0.35 g of SEP, SBA, or their corresponding silver- and copper-loaded materials were dispersed in 5 g of distilled water by vigorous stirring. Afterwards, 5 g of acetone were added and the suspension sonicated for 30 s using an ultrasonic probe VC505 (500 W, Sonics and Materials Inc.) at 20% amplitude. The suspension was then mixed with the aforementioned CA solution in the proportion required to get 0.47 g of particles per gram of CA (5 wt.% of particles with respect to the total amount of CA and particles). Before electrospinning the final mixture was sonicated for another 30 s followed by 15 min of magnetic stirring. The electrospinning equipment consisted of a Heinzinger LNC 30000 high voltage power supply (0–30 kV, 0–2 mA), a Harvard PHD 22/2000 syringe pump and a flat collector (16 cm × 16 cm aluminum grid). The electrospinning mixture was transferred to a 5 mL syringe with a 23-gauge stainless steel blunt-tip needle at its end, which was connected to the high voltage power supply to create the required electric field. The parameters used were in all cases as follows: distance from needle tip to collector 15 cm, voltage used 23 kV and flow rate of polymer solution 0.8 mL/h.

2.3. Analytical methods

The morphological characterization of nanofibers was performed using scanning electron microscopy (SEM) from Carl Zeiss DSM 950 at an accelerating voltage of 10 kV. Scanning electron microscopy/energy dispersive X-ray spectroscopy (SEM/EDS) analyses were performed on a Hitachi TM-1000 Equipped with an EDS analysis system. A process of dehydration and drying with ethanol was carried out prior to analyzing fungi and colonized fibers by SEM. Transmission electron microscopy (TEM) images were obtained using a JEOL JEM-1010 transmission electron microscope at an accelerating voltage of 100 kV. Scanning electron micrographs (SEM) were acquired in a Hitachi TM-1000 apparatus. The conductivity and viscosity of electrospinning polymeric and precursor solutions was determined using a conductivity meter (model HI 4521) from Hanna Instruments and a rotational rheometer Bohlin Gemini nano from Malvern Instruments equipped with 40 mm cone and plate fixtures, respectively.

Nitrogen adsorption isotherms were recorded at 77 K in a Beckman-Coulter SA3100 apparatus on samples outgassed overnight at 200 °C. Small and wide-angle powder XRD patterns of SBA and metal-loaded SBA were obtained using an X-ray diffractometer Polycrystal X'pert Pro PANalytical, which employed Ni-filtered Cu Kα (k = 1.5406 nm) radiation and operated at 0.02/min, 40 kV and 40 mA. Inductively Coupled Plasma-Mass Spectrometry analyses (ICP-MS) were performed on a Perkin-Elmer NexION 300XX apparatus operating for solids after complete dissolution in hot acid media and on a Thermo Scientific ICP-MS model X Series 2. Particle size was measured by DLS using a Malvern Zetasizer instrument. A fluorometer/luminometer Fluoroskan Ascent FL and a Leica Microsystems Confocal SP5 fluorescence microscope were used to record the fluorescence emitted by the staining of fungi.

2.4. Fungistatic bioassays

The antifungal activity of functionalized fibers was evaluated using *A. niger* as probe species. The culture stock of *A. niger* spores was obtained from Leibniz-Institut DMSZ (German Collection of Microorganisms

and Cell Cultures, ATCC 6275). Spores were suspended in a saline solution (NaCl 0.9% w/v) and then cultivated at 24 °C ± 1 °C in Petri dishes using the malt extract agar medium (MEA): malt extract 30 g/L, soy peptone 3 g/L and agar 15 g/L, pH 7.0 (International Organization for Standardization, 2008). Fungi were grown for 21 days until the formation of mycelia and spores. Some spores were then carefully removed from the surface with saline solution and then centrifuged to eliminate the supernatant. The spores were resuspended, serially diluted and cultivated to obtain the desired stock concentration. Finally, the stock culture was stored in aliquots at − 20 °C in a 10% v/v glycerol solution with a concentration of 4×10^7 spores/mL. The reactivation of *A. niger* was carried out by twice adding 1 mL of medium to the Eppendorf containing the defrost fungi strain. The resulting 2 mL suspension was used to prepare the 1:10 dilutions used in the bioassays as indicated below.

The microbiological test consisted of two different assays with positive and negative controls to ensure optimal conditions and was performed in at least three independent measurements. First, the electrospun membranes bare and loaded with particles were exposed to *A. niger* as follows. Pieces of 2 cm^2 of the membranes were placed in 24-well plates with 20 μL of the 1:10 dilution of *A. niger* spores and led to a final volume of 2 mL with culture medium. Then, spores were incubated for 24 h at 21 °C, after which a spot of 50 μL of the spores in contact with fibers was placed in the middle of a Petri dish with MEA medium and cultured 24 h at 37 °C and 48 h more at 21 °C. This procedure allowed for the radial growth of *A. niger* avoiding extensive contact of hyphae with membranes or particles and limited the excessive growth that takes place at the optimum temperature for *A. niger*, which is in the 35–37 °C range. A commercial cellulose acetate membrane from Sartorius, 0.45 μm was also tested for comparison.

In another set of assays, the antifungal activity of the particles without any matrix or support (SBA, SEP and their metal-loaded forms) was tested. To this end, a prescribed amount of the dry material was carefully weighed and suspended in culture media to reach a final concentration of 100 mg/L. 20 μL of 1:10 dilution of spores of *A. niger* were used under the same conditions described before for the testing of fibers.

Radial growth is a widely used indicator of the ability of fungi to develop and spread and is usually expressed as colony diameter or radial growth rate (Parra and Magan, 2004). Growth assessment was performed using digital image analysis. Every image was digitally treated to count pixels, which were converted to surface, using the public domain Java image processing software ImageJ.

FUN-1 staining was performed as follows. 200 μL aliquots of the incubated (24 h, 21 °C) spores were transferred to the wells of 96-well plates and kept 24 h at 37 °C to ensure the fungi passing to micellar phase. The staining was performed dissolving 60 μL of FUN-1 in 940 μL of dimethyl sulfoxide (DMSO) and 10 μL of the mixture was added to each well. Readings were performed at 30 °C. Hydrogen peroxide was used as positive control.

3. Results and discussion

3.1. Characterization of particles and nanofibrous membranes

The nitrogen adsorption–desorption isotherms of the particle materials are shown in Fig. S2 (SI). SBA and metal-loaded SBA exhibit type IV isotherms according to IUPAC classification with H1 hysteresis loop (Fig. S2-A), which is characteristic of mesoporous materials with one-dimensional cylindrical channels. SEP displays a type V isotherm with capillary condensation. Surface areas were 731 m^2/g for SBA, 377 m^2/g for Ag/SBA and 643 m^2/g for Cu/SBA with mean pore diameter in the 5–8 nm calculated using the Barrett–Joyner–Halenda (BJH) method on the desorption branch. Surface area of SEP was 242 m^2/g, whereas for Ag/SEP and Cu/SEP were 72 m^2/g and 49 m^2/g respectively, with a much broader pore structure. The decrease in surface area after metal loading was due to pore clogging and the partial breakdown of the pore structure upon calcination, but it did not suppose an obstacle for using the loaded material as a metal reservoir.

The low-angle XRD diffraction pattern of Ag/SBA and Cu/SBA are shown in Fig. S3-A and B (SI). Both present three well-resolved diffraction peaks which correspond to (100), (110) and (200) planes, and reflect the hexagonally ordered (p6mm) structure of SBA-15 (Khodakov et al., 2005). The powder XRD patterns in the wide-angle region (Fig. S3-C and D) show broad diffraction peaks at 2θ = 24°, which correspond to the amorphous nature of SBA-15 (Prathap et al., 2012). The XRD pattern of Cu/SBA matches the peaks of the monoclinic CuO (Ethiraj and Kang, 2012). No evidence of metal copper was observed as the planes of fcc structure of copper (100), (200) and (220) at 2θ 43.0°, 50.1° and 73.5° (JCPDS No. 85-1326) were absent from XRD patterns. The XRD pattern of Ag/SBA showed a strong peak at 2θ = 38.1° and peaks at 44.4°, 64.5° and 77.4° corresponding to the diffractions of (111), (200), (220) and (311) reflections of the face cantered cubic (fcc) structure of metallic silver. Silver oxide peaks do not appear as Ag_2O decomposes into metallic Ag at 473 K. Fig. S1 shows electron micrographs of SEP and SBA bare and metal-loaded particles. SEP images indicate good defibrillation with individual fibers clearly observed in all samples. The absence of visible aggregates in CA fibers suggests a homogeneous distribution as expected from their interaction with polymers capable of hydrogen bonding (Dasari et al., 2012).

Fig. S4A (in SI) shows CA electrospun membranes displaying well-defined fibers without beading and showing no evident flaws. The mean fiber diameter of neat CA fibers was 593 nm as determined from at least 50 measurements on SEM images. Fig. S5 (SI) displays histograms with the distribution frequency of fiber diameters for the different electrospun membranes, also taken from SEM images. The mean diameter of particle loaded fibers ranged from 425 to 536 nm, roughly 10–20 % lower than neat CA fibers and with considerably higher proportion of thinner fibers. This was interpreted as a consequence of the higher conductivity of the electrospinning mixture, which is associated with lower fibre diameters (Bhardwaj and Kundu, 2010).

SBA and metal-loaded SBA particles are shown in Fig. S4B and in Fig. 1A–B in which silica appeared entrapped within fibers, reasonably well dispersed and occasionally forming aggregates in the micrometre range (insets in Fig. 1A–B). Fig. 1C–D corresponds to fibers bearing metal-loaded SEP particles, in which there were no evident particle aggregates. (CA-SEP is shown in Fig. S3, SI). The shape of SBA particles does not exclude their presence in fibers independently from the visible aggregates as the smaller axis of SBA particles is in the order of magnitude of fibre diameter. The presence of metals in electrospun membranes was confirmed by chemical microanalysis using energy dispersive X-ray spectroscopy (EDS). The results are shown in Fig. S6 (SI).

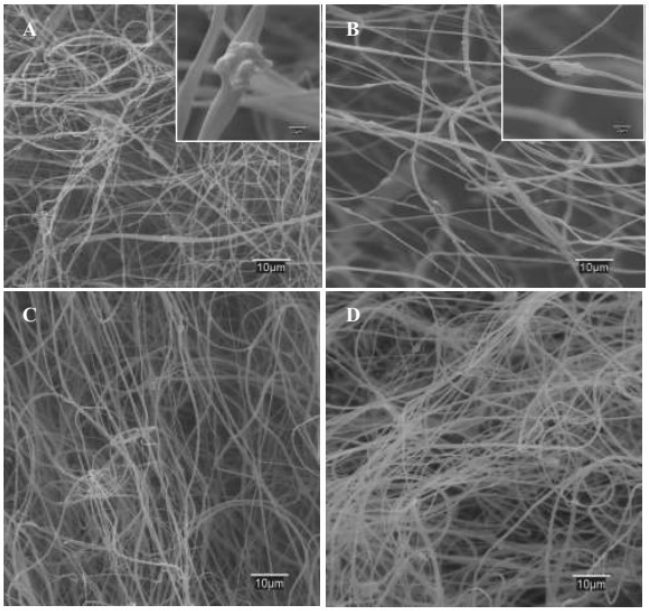

Figure 1. SEM electrospun membranes of (A) CA-Ag/SBA, (B) CA-Cu/SBA, (C) CA-Ag/SEP and (D) CA-Cu/SEP (insets: detail of fibers with entrapped particles; images of neat CA fibers, CA-SBA and CA-SEP are given as Supplementary information).

3.2. Antifungal performance

Fungal spores placed in a suitable environment germinate allowing fungal growth in branching filaments called hyphae (Pazouki and Panda, 2000). *Aspergilli* normally grow on solid substrates developing radial symmetrical white macro-colonies, which occasionally develop yellow tinges on which dark brown conidiophores are eventually formed as shown in Fig. S7 (in SI) (Dijksterhuis and Wösten, 2013). We found that during the first 24 h at 21 °C in MEA medium the germinating conidia started to change, but it was not until 24 h after raising the temperature to 37 °C that the first stalks of *A. niger* become apparent (Fig. S8-A in SI). Conidiophores clearly appeared 72 h post-inoculation, SEM micrographs showed that once the stalk has reached its maximum height, the tip swells and forms a vesicle with a diameter of 10 μm approx. (Fig. S8-B). In biserate species such as *A. niger*, the vesicle surface buds, resulting in metulae and conidia (Fig. S8-C and D in SI). As a result, more than 10^4 conidia can be produced per conidiophore.

Fig. 2 shows daily pictures of *A. niger* cultured for 72 h after being exposed to the different particles. *Aspergillus* produces black or brown conidia during maturation (Fig. S8-C), a phase that took place in control cultures after 24 h at 21 °C followed by 24 h in MEA at 37 °C. Morphological changes were not apparent in fungi cultured after contact with SBA or SEP but were clear for metal-loaded particles (Fig. 2). In the case of spores in contact with copper and silver, fungi split in several colonies losing its characteristic radial form such as that shown in Fig. S7-A and in the first column of Fig. 2. This evolution was particularly clear for silver-loaded particles. For the case of Cu/SBA and Cu/SEP an accelerated maturation of conidiophores was also apparent, the black color of conidia being clearly visible after only 24 h. Pictures at 48/72 h show abundant black conidia forming several subcolonies. The effect of copper inducing conidiation has been described elsewhere (Adams et al., 1988). It is important to note that the particles were in contact 24 h (21 °C) with germinating spores but absent during all the growth phase, so the images represent the damage produced before the formation of conidiophores.

The comparison of radial growth for spores in contact with the different materials during 24 h is shown in Fig. 3. The areas correspond to that reached by the fungus after 72 h following the 24 h period of contact with particles and were obtained from digital image processing as indicated above. The control corresponds to MEA medium without any particle and it is within the mycelium expected growth for *A. niger* under optimal conditions (Lee and Adams, 1994). Bare SBA and SEP had an effect on the growth rate and the surface occupied by the fungus. This could be due to the adsorption of micronutrients or the ion exchange of minerals. Specifically, SEP can exchange Mg^{2+} with dissolved metals and it is important to note that no solution of trace metals nor nutrient supplement was added to the culture media. Another possible reason is the interference of particles with the first stages of mycelium growth as discussed below for the effect of non-metal loaded fibers. The asterisks in the figure

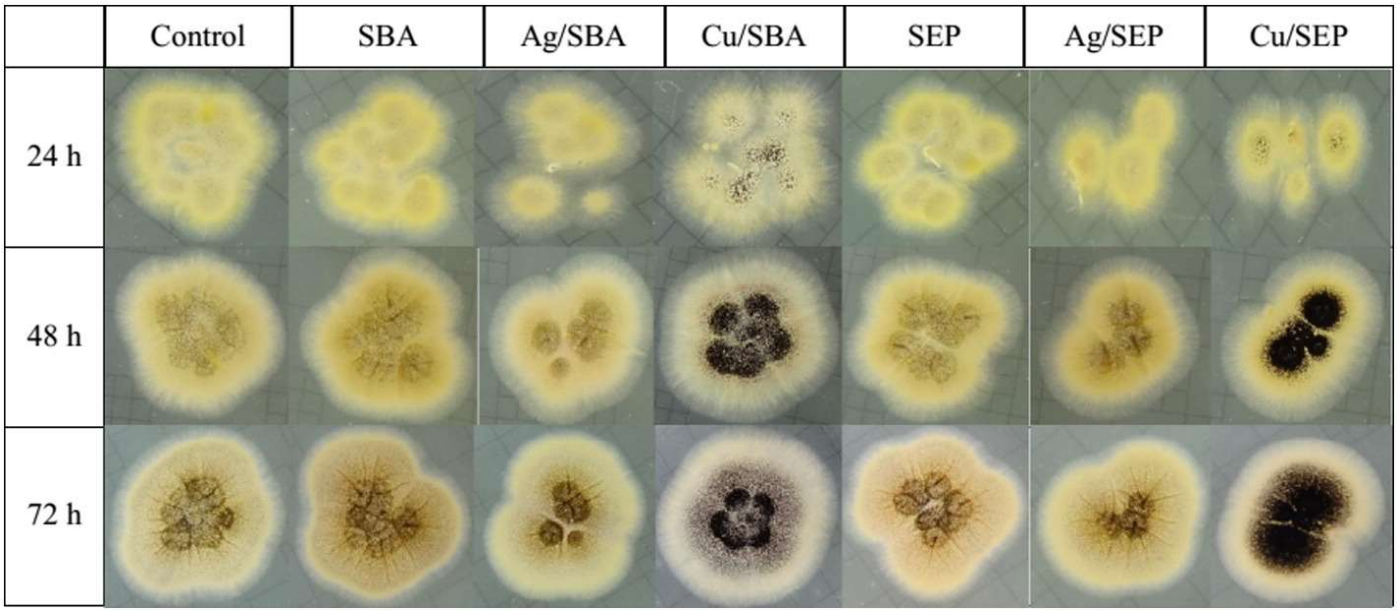

Figure 2. *A. niger* cultured from spores exposed for 24 h to different particles.

mark the cases for which metal-loaded particles were significantly more effective in reducing fungal growth than the corresponding bare particles. This was the case of Ag/SBA and Cu/SBA, with reductions of ~ 40% with respect to SBA and ~ 65% relative to MEA, particle-free, controls.

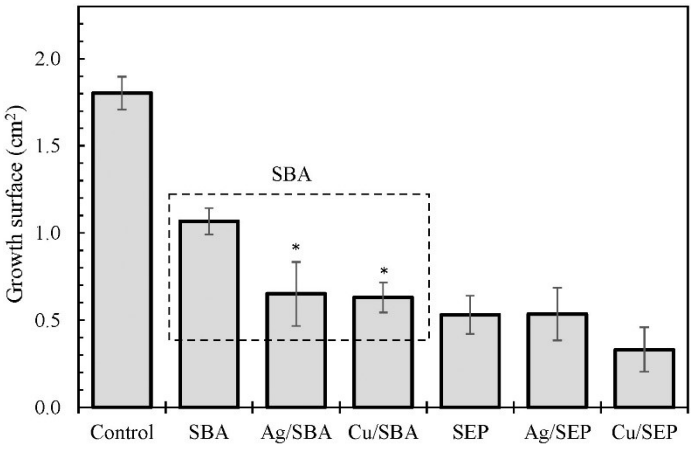

Figure 3. *A. niger* growth area after 72 h (24 h at 37 °C and 48 h at 21 °C) when germinating spores were previously in contact with particles (100 mg/L) during 24 h (21 °C). The asterisks mark the experiments for which metal-loaded particles induced significantly lower growth than the same non-loaded material.

The effect of particles on fungal viability was also assessed using FUN-1 staining. FUN-1 is a two-color fluorescent viability staining of fungi, which passively diffuses into the cytoplasm yielding a uniformly distributed green fluorescence. Subsequent processing of the dye by healthy cells results in vacuolar structures that exhibit red fluorescence. The formation of such intravacuolar structures requires plasma membrane integrity and full metabolic capability, while dead cells fluoresce yellow–green, without red signal. A confocal image of the double-staining of hyphae is shown in Fig. S9 (SI). Fig. 4 shows the damage to the hyphae after contact with the particles as a decrease in the red fluorescence recorded in the 542–592 nm interval. The results correspond to spores in contact 24 h with particles, after which 200 μL of them were transferred to 96-well plates for 24 h at 37 °C in order to produce the micellar phase before staining. The results are given in fluorescence units relative to the average of control runs and are generally coincident with fungal growth data. Fungi in contact with Ag/SBA and Cu/SBA gave rise to significantly lower viability readings with respect to controls and bare SBA particles. An asterisk represents the experiments for which metal-loaded particles induced significantly lower growth than the same non-loaded material. As in growth area measurements, Cu/SEP displayed the lower viability of all runs, also significantly below the effect of SEP alone.

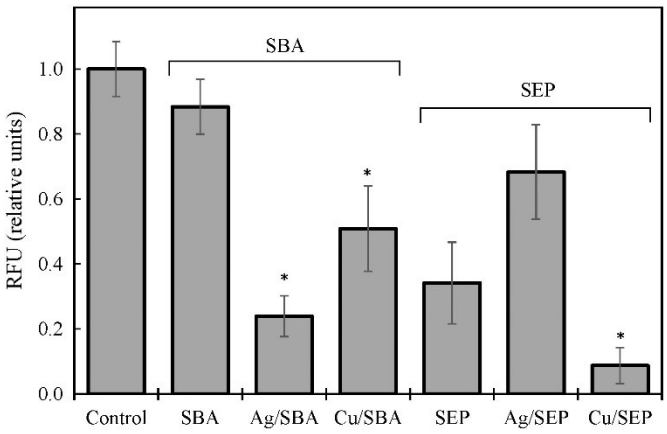

Figure 4. RFU signal for FUN-1 staining of hyphae after 24 h at 37 °C when germinating spores were previously in contact with particles (100 mg/L) during 24 h (21 °C). The asterisks mark the experiments for which metal-loaded particles induced significantly lower growth than the same non-loaded material.

The effect of particles entrapped in CA membranes on the subsequent growth of fungi was assessed in another series of runs, the results of which correspond to the pictures displayed in Fig. 5. The growth of *A niger* when colonizing electrospun membranes is illustrated with the SEM micrographs of Fig. S10 (SI), which shows hyphae and conidiophores entangled with CA fibers. It was apparent that the presence of copper (CA-Cu/SBA and CA-Cu/SEP) induced a rapid maturation and production of abundant black conidia as well as the formation of several subcolonies. The lower growth of *A. niger* was also clear after 24 h post-contact with CA-Ag/SBA and CA-Ag/SEP. The quantitative growth data are depicted in Fig. 6 as surface covered by fungi after 24 h at 37 °C followed by 48 h at 21 °C. The results were also significant for all metal-loaded particles present in membranes during the exposure of spores. A double asterisk marks the cases for which the results displayed a significantly lower growth than CA controls and membranes of the same particles in non-loaded form (bare SBA or SPE). This was the case of membranes including Ag/SBA and Cu/SEP, particularly the latter, which resulted in the highest growth inhibition of all tested membranes. With a single asterisk, the membranes including Cu/SBA and Ag/SEP yielded growths significantly lower than CA controls but not significantly below membranes spun with SBA and SEP, respectively. It is also interesting to note that the growth on CA and Commercial CA was lower than that of control runs with fungi covering roughly 50% less surface (Fig. 6). We think this may be a consequence of the interference of fibers with the growing mycelium. During the first stages of development, which starts forming clumps of aggregated hyphae that represent an intermediate stage before dispersed growth, fungi are considerably affected by substrate features (Krijgsheld et al., 2013).

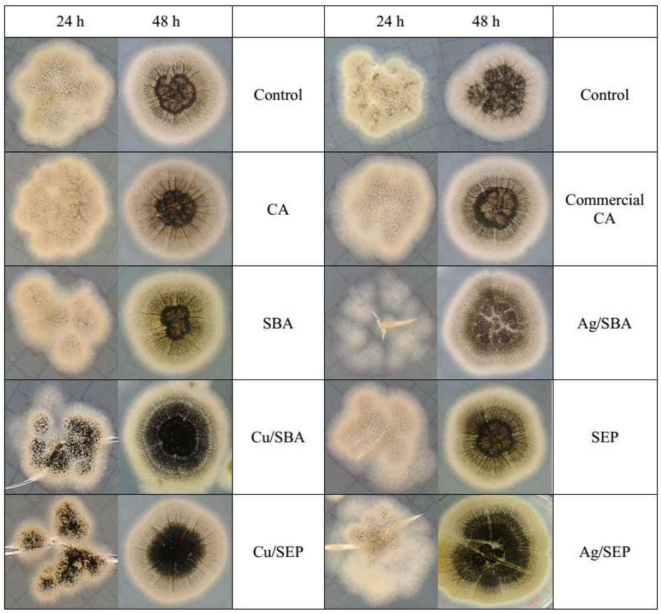

Figure 5. *A. niger* growth after contact for 24 h with neat or metal-loaded fibers. Culture conditions as indicated in the text.

The lower growth in the presence of CA incorporating non-metal loaded SBA and SEP fibers with respect to neat CA would support this assumption. In this case, the fibers were considerably thinner than those of pure CA, which would increase the interference with the first stages of mycelium growth (Fig. S5).

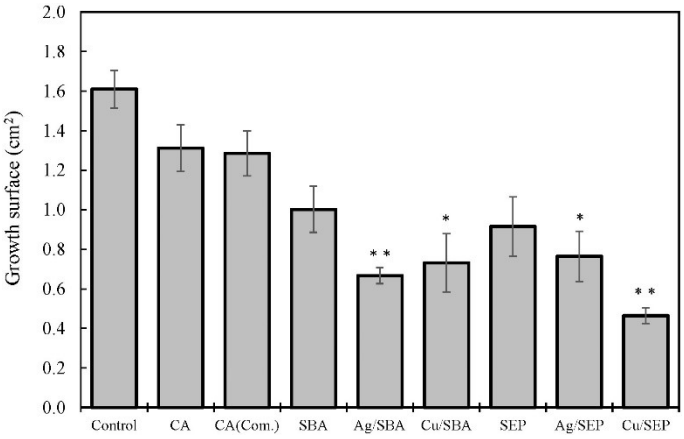

Figure 6. *A. niger* growth area after 72 h (24 h at 37 °C and 48 h at 21 °C) when germinating spores were previously in contact with electrospun membranes during 24 h (21 °C). One asterisk marks the experiments for which particle-loaded membranes induced significantly lower growth than CA control. Two asterisks mark cases for which metal-loading induced significantly lower growth than the same bare particles.

The results showed that the exposure of spores to particles during germination influenced the subsequent growth of *A. niger* in the absence of further contact with metals after the first 24 h. This is consistent with what is known about the biology of *A. niger*. It has been shown that dormant conidia of *A. niger* change abruptly during the first hours of germination due to the need to initiate all the vital functions which include protein synthesis and respiration. It has also been proven that certain antifungals do not affect *A. niger* during the first 2 h of germination, but subsequent stages became effectively blocked with thorough changes of the transcriptome inside the cells (van Leeuwen et al., 2013).

The mode of action of metal nanoparticles is still controversial. Silver nanoparticles have been the most thoroughly studied system. The biocidal effect is known to be a consequence of direct membrane damage, ROS production, and block of respiration, induced by both nanoparticles and silver ions (Rizzello and Pompa, 2014). The role played by the nanoparticle and silver ions released from them has been studied by many authors. Experimental data, however, indicate that the antimicrobial activity of silver nanoparticles is only due to the release of silver ions, with negligible effect due to direct particle contact (Xiu et al., 2012). The biocidal effect of copper nanoparticles has also been attributed to the release of copper ions, which are responsible for the disruption of several critical biochemical processes (Stohs and Bagchi, 1995, Ruparelia et al., 2008). Therefore, avoiding direct contact between cells and

nanoparticles does not limit their biocidal effect. Conversely, it is a straightforward way of preventing the dissemination of nanoparticles into the environment. The release of metal ions is dealt with in the following section.

3.3. Metal release

The role of metal-loaded particles as a reservoir for the release of cations is supported by ICP-MS data, which are shown in Fig. 7 expressed in mg/100 mg of particles or mg/g mat after 24/72 h in contact with MEA or water. Silver loaded particles in contact with water released up to 2.9 μg/g and 3.5 μg/g for SBA and SEP, respectively, during the first 24 h. The corresponding amount of copper released for supported copper materials was 4.3 μg/g (Cu/SBA) and 5.4 μg/g (Cu/SEP). In view of the higher metal loading of SEP, these results suggest an important influence of the higher surface area and mesoporous structure of SBA on the rate of metal release. When using MEA instead of water (Fig. 7), the amount of metals in solution was lower, probably as a consequence of the different fate of metals in complex biological media, particularly silver in the presence of chloride (Mukherjee et al., 2011).

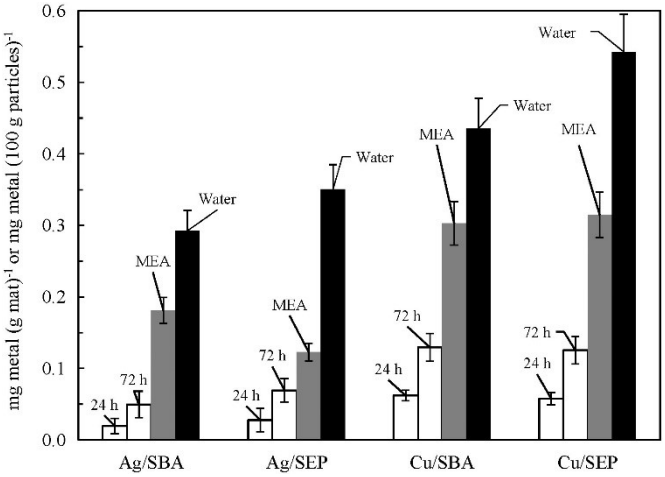

Figure 7. Amount of metal released by particles in contact with MEA or water (24 h, dark bars) and for metal-loaded membranes in contact with MEA during 24/72 h.

The speciation of dissolved species, obtained using visual MINTEQ (version 3.1, KTH, Stockholm, Sweden) showed that the equilibrium distribution in aqueous solution is dominated by Ag^+ in the case of silver and a series of hydroxylated species in the case of copper, mainly $Cu_2(OH)_2^{2+}$, $Cu_3(OH)_4^{2+}$ and Cu^{2+}, which is consistent with the results reported elsewhere (Quirós et al., 2015b). The higher amount of metal released for Ag/SBA and Cu/SEP was in good agreement with the results of FUN-1 staining shown in Fig. 4 and with the *A. niger* growth area shown in Fig. 6. The amount of metals put in solution by membranes in contact with MEA (Fig. 7) showed a daily metal release that represented roughly 1 % of the total amount of loaded silver or copper for materials supported in SBA (1.1 % for Ag/SBA and 1.4 % for Cu/SBA) with lower figures for SEP supported materials (0.23 % and 0.62 % for Ag/SEP and Cu/SEP, respectively) in line with the results obtained for free particles. The amount of copper released was slightly larger than that of silver, which is probably a consequence of metal speciation and the presence of chlorides. After the first 24 h the rate of release was somewhat lower due to the loss of the most accessible metal such as that deposited on particle surface. The average of metal loss during the second and third day in contact with MEA was 0.86 % and 0.76 % for Ag/SBA and Cu/SBA and 0.17 % and 0.37 % for Ag/SEP and Cu/SEP respectively. In all cases, the release during the first 24 h was slightly higher than the daily average of the two following days, which is most probably due to the presence of metals on particle surface or in highly accessible pores. It was also apparent that the encapsulation of metal nanoparticles in polymeric composites considerable reduced the rate of metal release to the solution, with a total amount of metal in solution typically one order of magnitude lower for membranes for the same time in contact with liquid medium. The durability of metal-loaded fibers is also linked with the nature of the metal. Copper in very low concentration is essential for the production of citric acid by *A. niger*. An excess affects the activity of membrane transport carriers associated with the excretion of citric acid by the mycelium and also inhibits several enzymes such as aconitase and isocitrate dehydrogenase (Tsekova et al., 2000). The results obtained reflect that the copper concentrations used in this study were sufficiently high to affect the fungal growth, but not to lead to conidia degeneration by accumulation of citric acid. In general, silver is more antibacterial than antifungal, particularly when comparing with *A. niger*, which is a particularly resistant strain (Kathiresan et al., 2010). Besides, the presence of oxygen is known to have a significant role in the release of silver ions from silver nanoparticles. The decrease of dissolved oxygen due to the metabolic activity of fungi would be another reason for explaining the relatively good results of copper in comparison with silver (Liu and Hurt, 2010).

4. Conclusions

CA electrospun composites prepared with SBA and SEP formed well-defined fibers without beading and flaws with a diameter in the 400–500 nm range. SBA, SEP and their corresponding metal-loaded nanomaterials became entrapped within the fibers and well dispersed with occasional aggregates randomly distributed along the fibers.

The growth of *A. niger* was significantly impaired when spores were in contact with metal-containing nanomaterials during germination (24 h). All metal-loaded particles led to a significantly lower surface occupied by fungi with respect to controls with an average of 70% reduction both for copper and silver

materials. All metal containing particles also reduced the fungal metabolic activity measured using FUN-1 readings. The effect on fungal growth and metabolic activity was particularly important for Cu/SEP, which can be attributed to its higher metal loading and release.

All metal-loaded CA composite membranes significantly impaired the growth of *A. niger*. The results showed that the exposure of spores to particles and CA composites during germination negatively influenced the subsequent growth of *A. niger*. In the case of copper nanomaterials, an accelerated maturation of conidiophores was observed, with black conidia being clearly visible after only 24 h. Nanometal-containing particles acted as a reservoir for the controlled release of cations. The amount of metals released daily by CA composite membranes represented roughly 1% of the total amount of silver or copper.

Acknowledgments

Financial support for this work was provided by the FP7-ERA-Net Susfood, 2014/00153/001, the Spanish Ministry of Economy and Competitiveness, CTM2013-45775 and the Dirección General de Universidades e Investigación de la Comunidad de Madrid, Research Network S2013/MAE-2716. One of the authors, J.Q., thanks the University of Alcalá for the award of a pre-doctoral grant.

References

Adams TH, Wieser JK, Yu JH. Asexual sporulation in *Aspergillus nidulans*. Microbiol Mol Biol Rev 1988, 62:35–54.

Al-Ashhab A, Herzberg M, Gillor O. Biofouling of reverse osmosis membranes during tertiary wastewater desalination: microbial community composition. Water Res 2014, 50:341-349.

Baker JS, Dudley LY. Biofouling in membrane systems—A review. Desalination 1998, 118:81-89.

Bhardwaj N, Kundu SC. Electrospinning: a fascinating fiber fabrication technique. Biotech. Adv. 2010, 28:325-347.

Botequim D, Maia J, Lino MMF, Lopes LMF, Simoes PN, Ilharco LM, Ferreira L. Nanoparticles and surfaces presenting antifungal, antibacterial and antiviral properties. Langmuir 2012, 28:7646-7656.

Campoccia D, Montanaro L, Arciola CR. A review of the biomaterials technologies for infection-resistant surfaces. Biomaterials 2013, 34:8533-8554.

Dasari A, Quirós J, Herrero B, Boltes K, García-Calvo E, Rosal R. Antifouling membranes prepared by electrospinning polylactic acid containing biocidal nanoparticles. J Memb Sci 2012, 405:134-140.

Dijksterhuis J, Wösten H. Development of *Aspergillus niger* Stud Mycol 2013, 74:1-29

Dobrzański LA, Hudecki A, Chladek G, Król W, Mertas A, Surface properties and antimicrobial activity of composite nanofibres of polycaprolactone with silver precipitations, Arch Mat Sci Eng 2014, 70:53-60.

El-Newehy MH, Al-Deyab SS, Kenawy ER, Abdel-Megeed A, Fabrication of electrospun antimicrobial nanofibres containing metronidazole using nanospider technology, Fibres and Polymers 2012, 13:709-717.

Esteban-Cubillo A, Pina-Zapardiel R, Moya JS, Barba MF, Pecharromán C. The role of magnesium on the stability of crystalline sepiolite structure. J Eur Cer Soc 2008, 28:1763-1768.

Ethiraj AS, Kang DJ. Synthesis and characterization of CuO nanowires by a simple wet chemical method. Nanoscale Res Lett 2012, 7:1-5

Falletta E, Bonini M, Fratini E, Lo Nostro A, Pesavento G, Becheri A, Lo Nostro P, Canton P, Baglioni P. Clusters of poly(acrylates) and silver nanoparticles: structure and applications for antimicrobial fabrics. J Phys Chem C 2008, 112:11758–11766.

Flannigan B, Samson RA, Miller JD. Microorganisms in home and indoor work environments, Taylor and Francis, 2011.

Greiner A, Wendorff JH. Electrospinning: a fascinating method for the preparation of ultrathin fibres. Angew Chem Int Ed, 2007, 46:5670-5703.

Grieger KD, Linkov I, Hansen SF, Baun A.Environmental risk analysis for nanomaterials: review and evaluation of frameworks. Nanotoxicology 2012, 6:196-212.

Hasan J, Crawford RJ, Ivanova EP. Antibacterial surfaces: the quest for a new generation of biomaterials. Trends Biotechnol 2013, 31:295-304.

Ignatova M, Stoilova O, Manolova N, Markova N, Rashkov I, Electrospun mats from styrene/maleic anhydride copolymers: Modification with amines and assessment of antimicrobial activity, Macromol Biosci 2010, 10:944-954.

Karthikeyan, K, Sowjanya RS, Yugandhar AD, Gopinath S, Korrapati PS, Design and development of a topical dosage form for the convenient delivery of electrospun drug loaded nanofibres, RSC Advances 2015, 5:52420-52426.

Kathiresan K, Alikunhi NM, Pathmanaban S, Nabikhan A, Kandasamy S. Analysis of antimicrobial silver nanoparticles synthesized by coastal strains of *Escherichia coli* and *Aspergillus niger*. Can. J. Microbiol. 2010, 56:1050–1059.

Khodakov AY, Zholobenko VL, Bechara R, Durand D. Impact of aqueous impregnation on the long-range ordering and mesoporous structure of cobalt containing MCM-41 and SBA-15 materials. Micropor Mesopor Mater 200, 579:29–39

Kim JR, Michielsen S, Photodynamic antifungal activities of nanostructured fabrics grafted with rose bengal and phloxine B against Aspergillus fumigatus, J Appl Polym Sci 2015, 132:42114.

Knetsch MLW, Koole LH. New strategies in the development of antimicrobial coatings: the example of increasing usage of silver and silver nanoparticles, Polymers, 2011, 3:340-366.

Krijgsheld P, Bleichrodt R, van Veluw GJ, Wang F, Müller WH, Dijksterhuis J, Wösten HAB. Development in Aspergillus. Stud Mycol 2103, 74:1-29.

Krishnan S, Weinman CJ, Ober CK. Advances in polymers for anti-biofouling surfaces. J Mater Chem 2008, 18:3405-3413.

Lakshminarayanan R, Sridhar R, Loh XJ, Nandhakumar M, Barathi VA, Kalaipriya M, Kwan JL, Liu SP, Beuerman RW, Ramakrishna S, Interaction of gelatin with polyenes modulates antifungal activity and biocompatibility of electrospun fibre mats, Int J Nanomed 2014, 9:2439-2458.

Lee BN, Adams TH. Over expression of flbA, an early regulator of Aspergillus asexual sporulation, leads to

activation of *brlA* and premature initiation of development. Mol Microbiol 1994, 14:323–334
Lipovsky A, Nitzan Y, Gedanken A, Lubart R. Antifungal activity of ZnO nanoparticles—the role of ROS mediated cell injury. Nanotechnology 2011, 22:105101.
Liu JY, Hurt RH. Ion Release kinetics and particle persistence in aqueous nano-silver colloids. Environ. Sci. Technol. 2010, 44:2169–2175.
Liu X, Lin T, Gao Y, Xu Z, Huang C, Yao G, Jiang L, Tang Y, Wang X. Antimicrobial electrospun nanofibres of cellulose acetate and polyester urethane composite for wound dressing. J Biomed Mater Res Part B 2012, 100B:1556–1565.
Mogensen JM, Frisvad JC, Thrane U, Nielsen KF. Production of Fumonisin B2 and B4 by *Aspergillus niger* on grapes and raisins. J Agric Food Chem 2010, 58:954-958.
Mukherjee P, Ahmad A, Mandal D, Senapati S, Sainkar SR, Khan MI, Parishcha R, Ajaykumar PV, Alam M, Kumar R, Sastry M. Fungus-mediated synthesis of silver nanoparticles and their immobilization in the mycelial matrix: A novel biological approach to nanoparticle synthesis. Nano Lett 2011, 1:515−519.
Nada AA, James R, Shelke NB, Harmon MD, Awad HM, Nagarale RK, Kumbar SG, A smart methodology to fabricate electrospun chitosan nanofiber matrices for regenerative engineering applications, Polym Adv Technol 2014, 25:507-515.
Palma N, Cinelli S, Sapora O, Wilson SH, Dogliotti E. Ochratoxin A-induced mutagenesis in mammalian cells is consistent with the production of oxidative stress. Chem Res Toxicol 2007, 20:1031-1037.
Panáček A, Kolář M, Večeřová R, Prucek R, Soukupová J, Krystof V, Hamal P, Zboril R, Kvítek L. Antifungal activity of silver nanoparticles against Candida spp. Biomaterials 2009, 30:6333-6340.
Pasricha A, Jangra SL, Singh N, Dilbaghi N, Sood KN, Arora K, Pasricha R. Comparative study of leaching of silver nanoparticles from fabric and effective effluent treatment. J Environ Sci 2012, 24:852-859.
Parra R, Magan N. Modelling the effect of temperature and water activity on growth of *Aspergillus niger* strains and applications for food spoilage moulds. J Appl Microbiol 2004, 97:429–438.
Paulo CS, Vidal M, Ferreira LS. Antifungal nanoparticles and surfaces. Biomacromolecules 2010, 11:2810-2817.
Pazouki M, Panda T. Understanding the morphology of fungi. Bioprocess Eng 2000, 22: 127-143.
Pfaller MA. Antifungal drug resistance: mechanisms, epidemiology, and consequences for treatment. Am J Med 2012, 125:S3-S13.
Pfaller MA, Pappas PG, Wingard JR. Invasive fungal pathogens: current epidemiological trends. Clin Infect Dis 2006, 43:S3-S14.
Pitt JI, Hocking AD. Fungi and food spoilage. Springer, 2009. Prathap MUA, Kaur B, Srivastava R. Direct synthesis of metal oxide incorporated mesoporous SBA-15, and their applications in non-enzymatic sensing of glucose. J Colloid Interface Sci 2012, 381:143–151.
Prucek R, Tuček J, Kilianová M, Panáček A, Kvítek L, Filip J., Kolář M, Tománková K, Zbořil R. The targetedScience of the Total Environment antibacterial and antifungal properties of magnetic nanocomposite of iron oxide and silver nanoparticles. Biomaterials 2011, 32:4704-4713.
Quirós J, Borges J, Boltes K, Rodea-Palomares I, Rosal R. Antimicrobial electrospun silver-, copper- and zinc doped polyvinylpyrrolidone nanofibres. J Hazard Mater 2015, 299:298–305.
Quirós J, Boltes K, Aguado S, de Villoria RG, Vilatela JJ, Rosal R. Antimicrobial metal–organic frameworks incorporated into electrospun fibers. Chem Eng J 2015, 262:189-197.
Rioux RM, Song H, Hoefelmeyer JD, Yang P, Somorjai GA. High-surface area catalyst design: synthesis, characterization, and reaction studies of platinum nanoparticles in mesoporous SBA-15 silica. J Phys Chem B 2005, 109:2192–2202.
Rizzello L, Pompa PP. Nanosilver-based antibacterial drugs and devices: mechanisms, methodological drawbacks, and guidelines. Chem Soc Rev 2014, 43:1501-1518.
Roe D, Karandikar B, Bonn-Savage N, Gibbins B, Roullet JB. Antimicrobial surface functionalization of plastic catheters by silver nanoparticles. J Antimicrob Chemother 2008, 61:869–876.
Ruparelia JP, Chatterjee AK, Duttagupta SP, Mukherji S. Strain specificity in antimicrobial activity of silver and copper nanoparticles. Acta Biomater 2008, 4:707-716.
Rzayev ZMO, Erdönmez D, Erkan K, Simsek M, Bunyatova U, Functional copolymer/organo-MMT nanoarchitectures. XXII. Fabrication and characterization of antifungal and antibacterial poly(vinyl alcohol-co-vinyl acetate/ODA-MMT/AgNPs nanofibers and nanocoatings by e-spinning and cspinning methods, Int J Polym Mater Polym Biomater 2014, 64:267-278.
Sharma D, Rajput J, Kaith BS, Kaur M, Sharma S. Synthesis of ZnO nanoparticles and study of their antibacterial and antifungal properties. Thin Solid Films 2010, 519:1224-1229.
Shi Y, Li Y, Zhang H, Yu Z, Yang D, Electrospun polyacrylonitrile nanofibres loaded with silver nanoparticles by silver mirror reaction, Mater Sci Eng C 2015, 51:346-355.
Sirelkhatim N, Lajeunesse D, Kelkar AD, Zhang L, Antifungal activity of amidoxime surface functionalized electrospun polyacrylonitrile nanofibres, Mater Lett 2014, 141:217-220.
Stohs SJ, Bagchi D. Oxidative mechanisms in the toxicity of metal ions. Free Radic Biol Med 1995, 18:321–336.
Sun LM, Zhang CL, Li P, Characterization, antimicrobial activity, and mechanism of a high-performance (-)-Epigallocatechin-3-gallate (EGCG)-Cu II/polyvinyl alcohol (PVA) nanofibrous membrane, J Agric Food Chem 2011, 59:5087-5092.
Tabe, S. Electrospun nanofibre membranes and their applications in water and wastewater treatment. In: Anming Hu and Allen Apblett (Eds.) Nanotechnology for Water Treatment and Purification, Springer International Publishing, 2014, p. 111-143.
Tonglairoum P, Ngawhirunpat T, Rojanarata T, Kaomongkolgit R, Opanasopit P, Fabrication of a novel scaffold of clotrimazole-microemulsion-containing nanofibres using an electrospinning process for oral candidiasis applications, Colloids Surf B 215, 126:18- 25.
Tsekova K, Dentchev D, Todorova D. Effect of Cadmium and Copper on the Production of Citric Acid by *Aspergillus niger*. Folia Microbiol. 2000, 45:331-334.
van Leeuwen MR, Krijgsheld P, Bleichrodt R, Menke H, Stam H, Stark J, Wösten HAB, Dijksterhuis J. Germination of conidia of *Aspergillus niger* is

accompanied by major changes in RNA profiles. Stud Mycol 2013, 74:59–70.
Wani IA, Ahmad T. Size and shape dependant antifungal activity of gold nanoparticles: a case study of Candida. Colloids Surf B 2013, 101:162-170.
Wang L, He H, Zhang C, Sun L, Liu S, Yue R. Excellent antimicrobial properties of silver-loaded mesoporous silica SBA-15. J. Appl. Microbiol. 2014, 116:1106-1118.
Xiao S, Shen M, Guo R, Wang S, Shi X. Immobilization of zerovalent iron nanoparticles into electrospun polymer nanofibers: synthesis, characterization, and potential environmental applications. J Phys Chem C 2009, 113:18062-18068.
Xiu ZM, Zhang QB, Puppala HL, Colvin VL, Alvarez PJ. Negligible particle-specific antibacterial activity of silver nanoparticles. Nano letters 2012, 12:4271-4275.

Supplementary Material

Electrospun cellulose acetate composites containing supported metal nanoparticles for antifungal membranes

Jennifer Quirós, Blanca Jalvo, Soledad Gonzalo, Karina Boltes, José Antonio Perdigón-Melón, Roberto Rosal*

Department of Chemical Engineering, University of Alcalá, 28871 Alcalá de Henares, Madrid, Spain.

* Corresponding author: roberto.rosal@uah.es

SUPPORTING INFORMATION

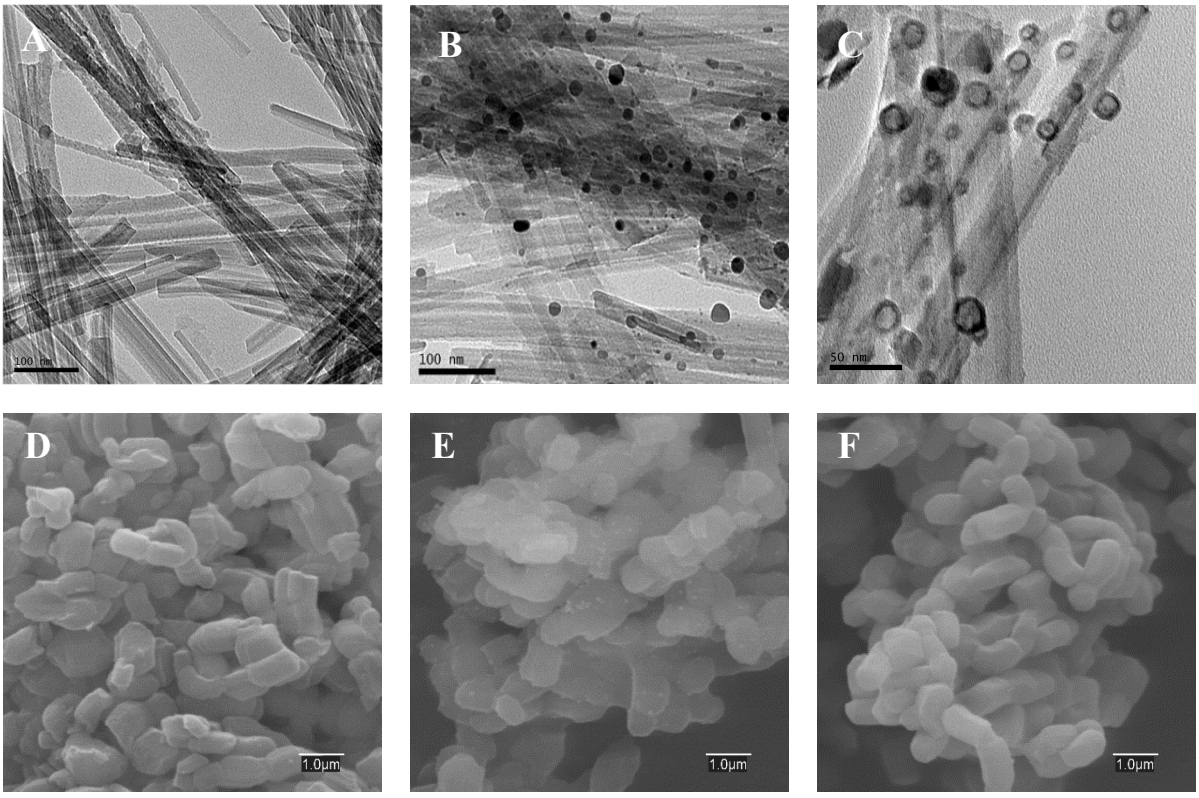

Fig. S1. TEM micrographs of SEP (A), Ag/SEP (B) and Cu/SEP (C) particles and SEM micrographs of SBA (D), Ag/SBA (E) and Cu/SBA (F) particles.

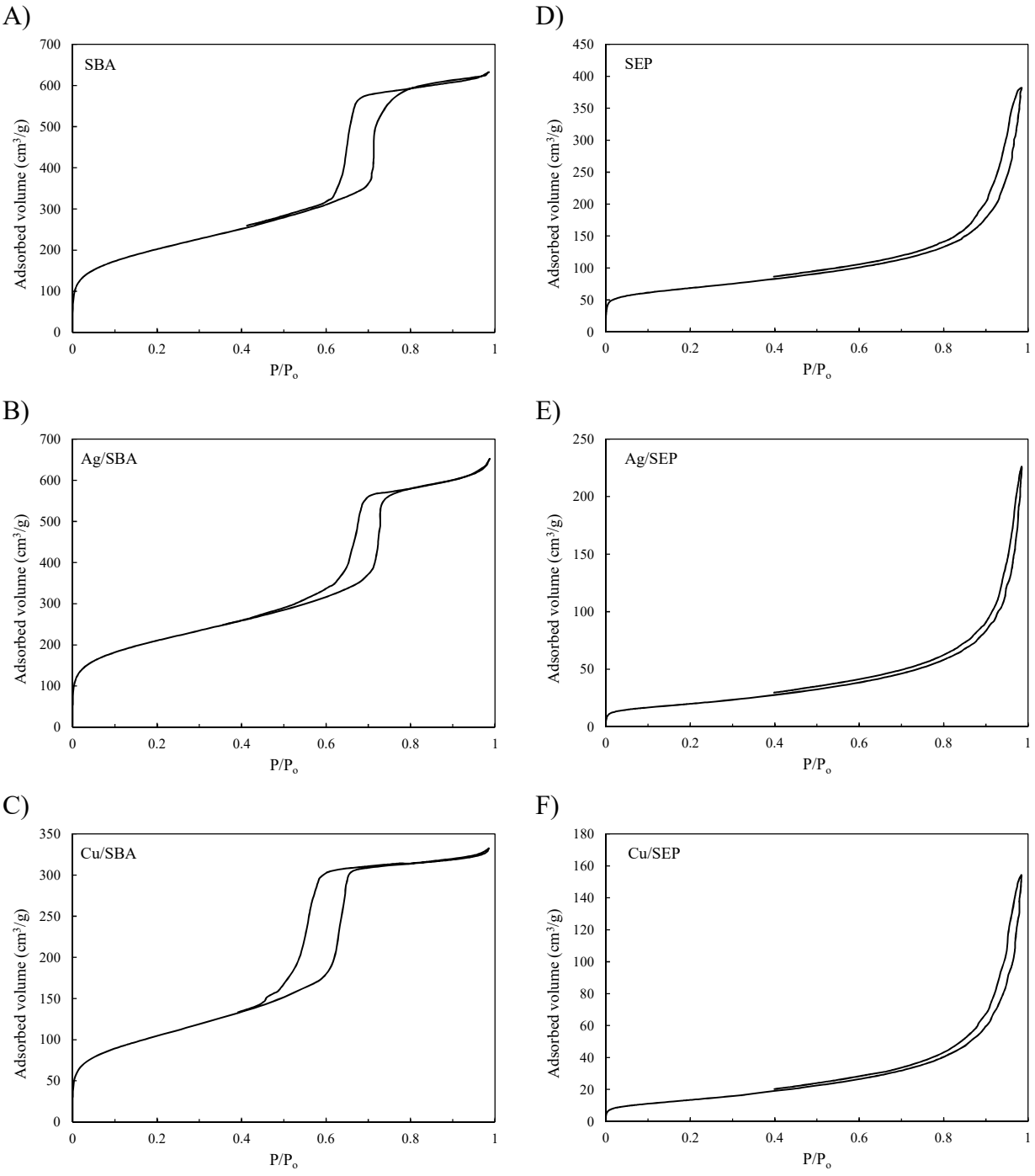

Fig. S2. Nitrogen adsorption desorption isotherm of (A) SBA, (B) Ag/SBA, (C) Cu/SBA, (D) SEP, (E) Ag/SEP and (F) Cu/SEP.

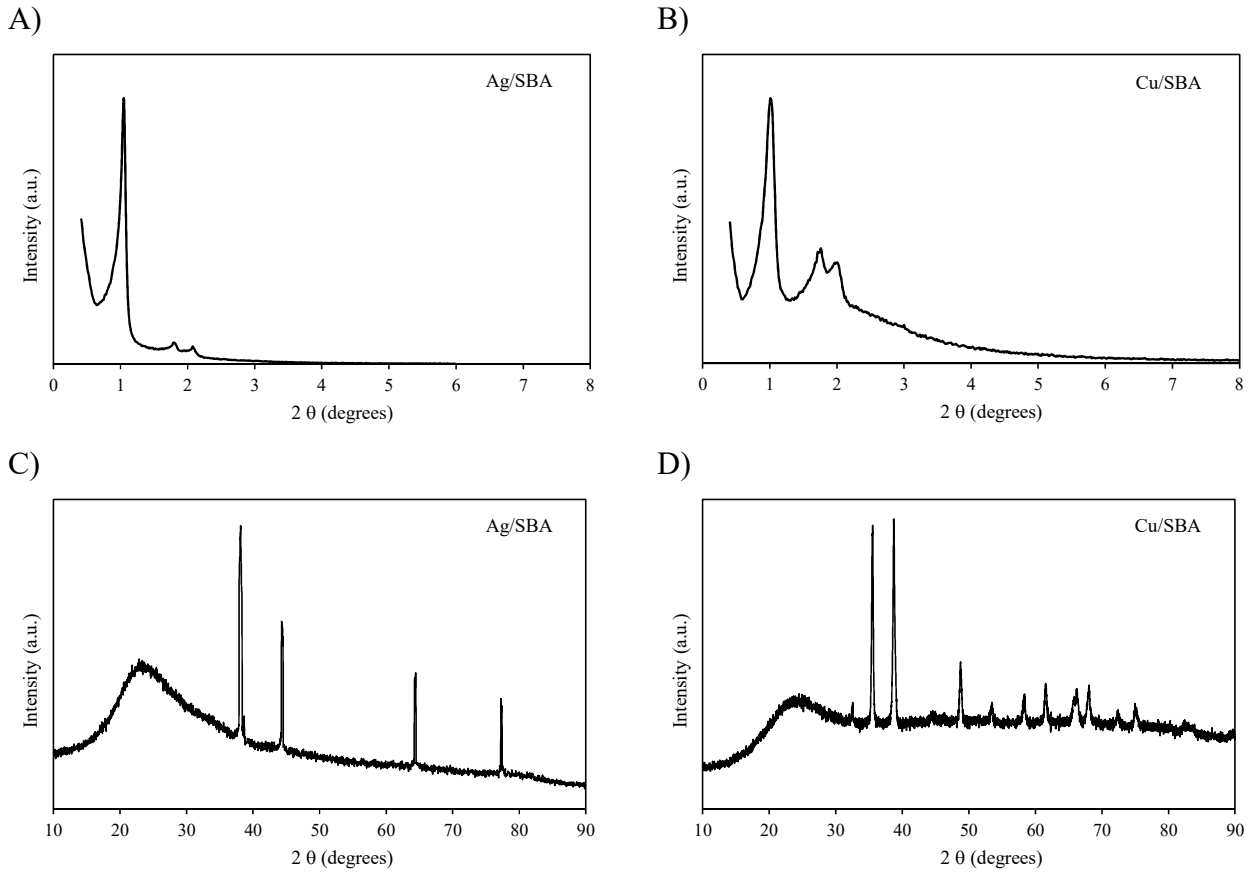

Fig. S3. Low-angle XRD pattern of Ag/SBA (A) and Cu/SBA (B). Wide angle XRD of Ag/SBA (C) and Cu/SBA (D).

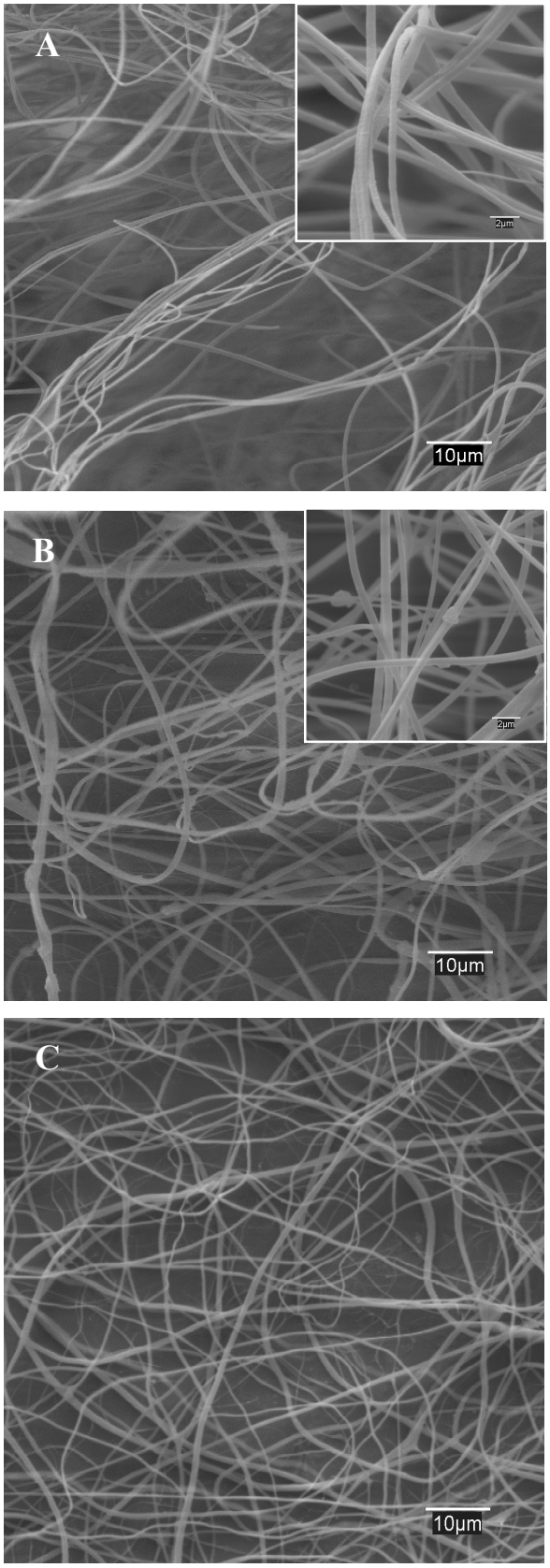

Fig. S4. SEM electrospun membranes of (A) neat CA, (B) CA-SBA and (C) CA-SEP.

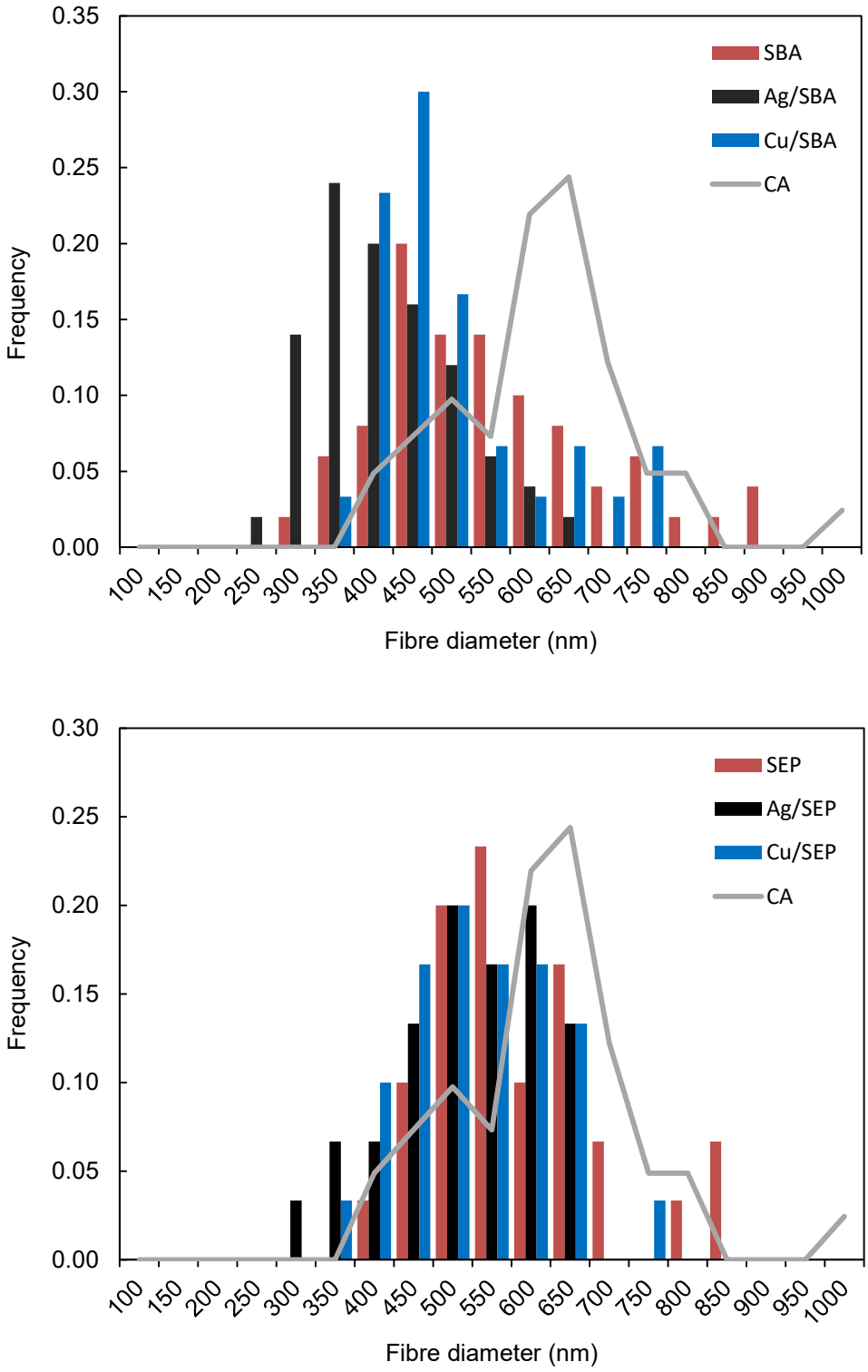

Fig. S5. Distribution frequency of fibre diameters for the different electrospun membranes.

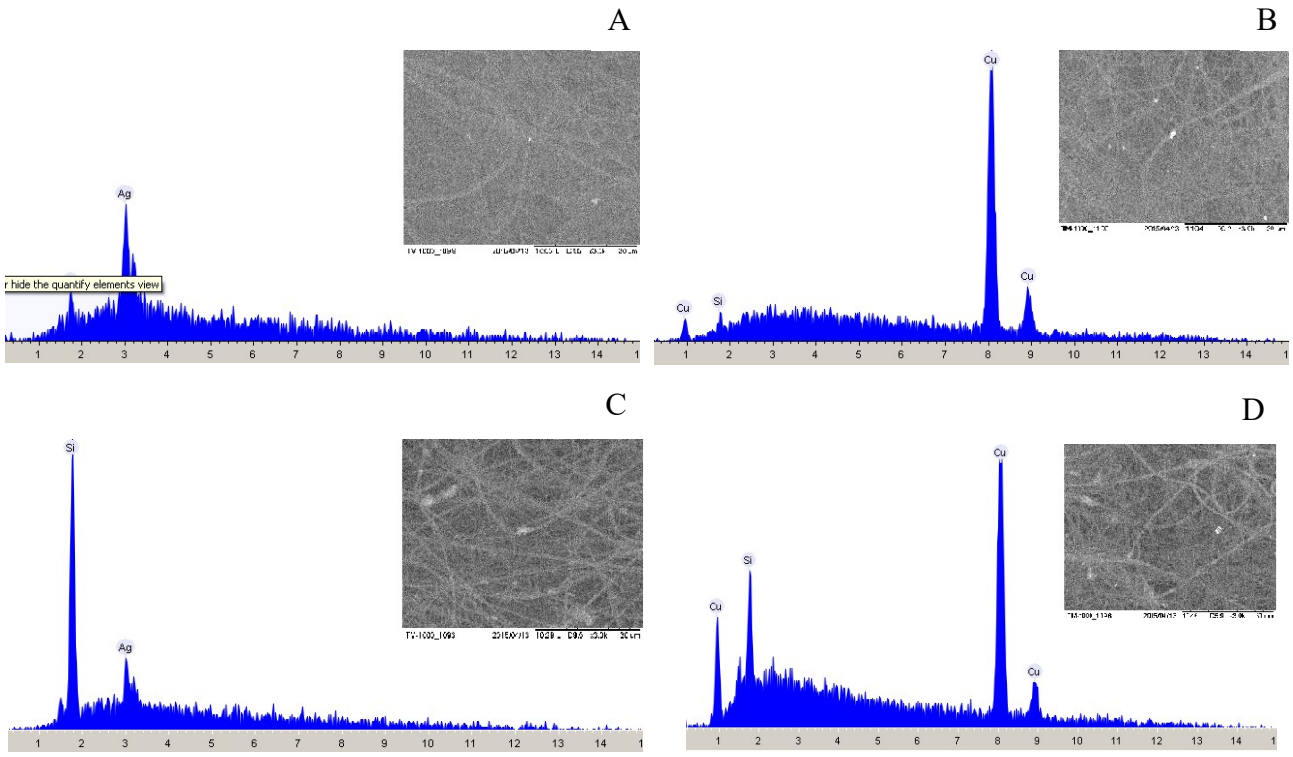

Fig. S6. SEM-EDS spectra of CA fibres loaded with Ag/SEP (A), Cu/SEP (B), Ag/SBA (C) and Cu/SBA (D).

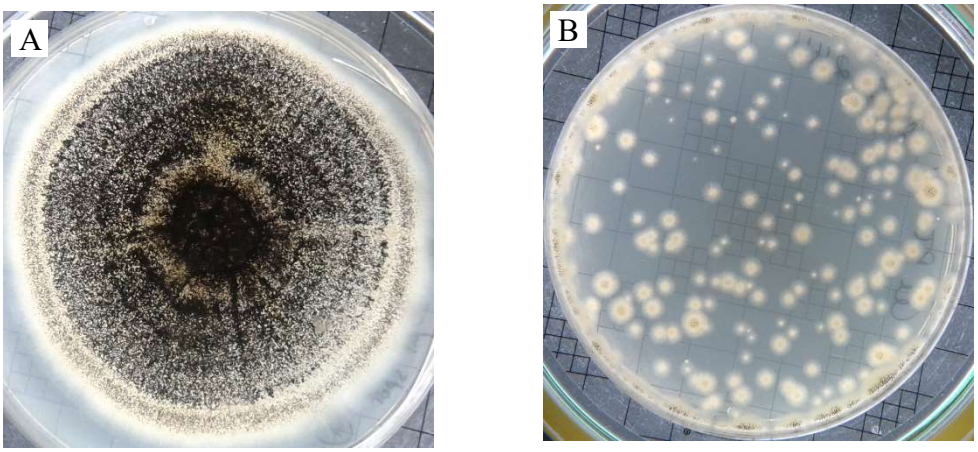

Fig. S7. Radial growth (A) and colonies (B) of *A. niger.*

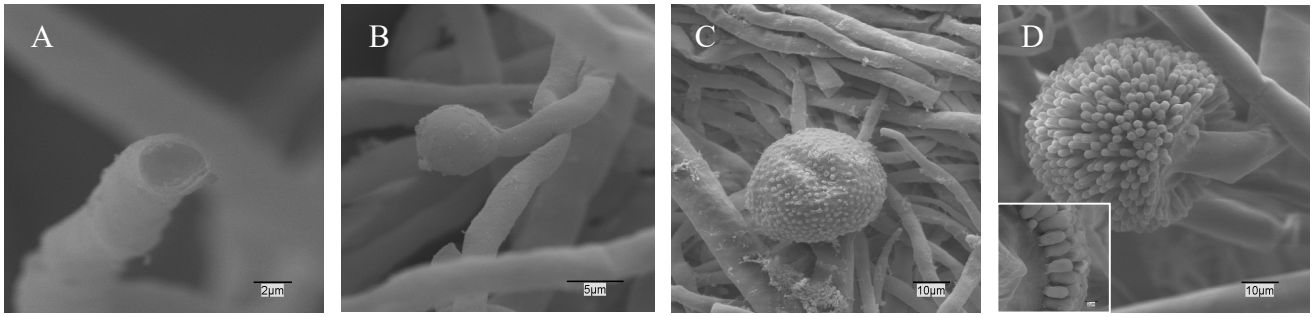

Fig. S8. Development of *A. niger* monitored by SEM. (A) hyphae, (B) vesicle (C) buds formed on the vesicle (D) metulae.

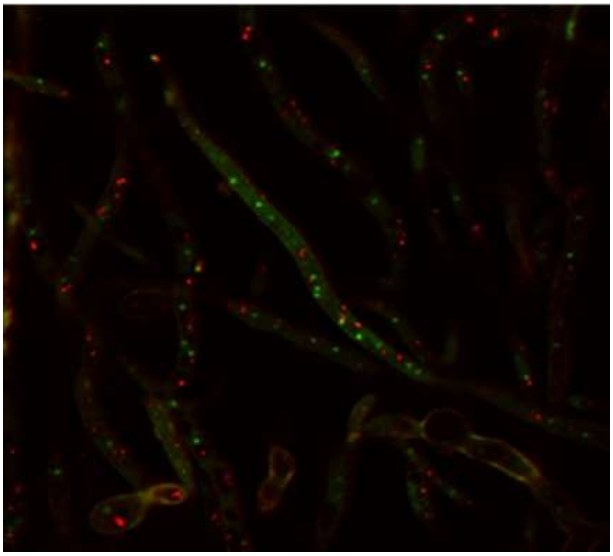

Fig. S9. Confocal micrograph of hyphae *A.niger* stained with FUN-1.

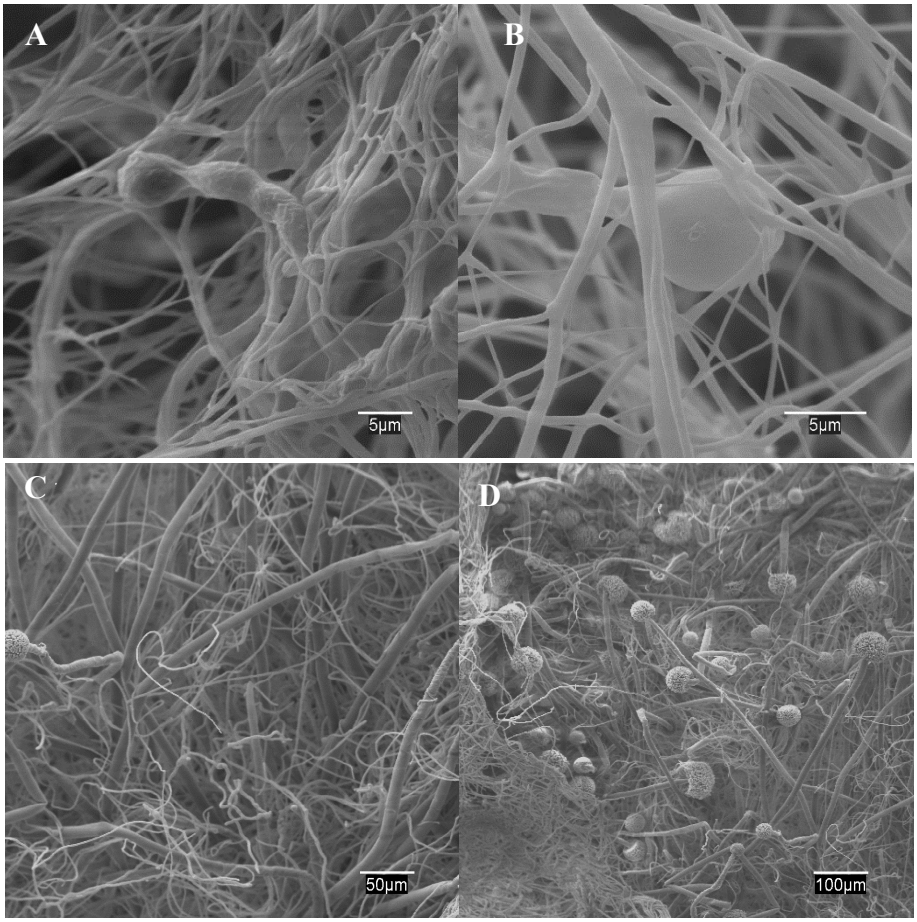

Fig. S10. *A. Niger* colonization of CA fibres.